



## RESEARCH ARTICLE

WILEY

# Suspended-sediment response to wildfire and a major post-fire flood on the Colorado Front Range

Sandra E. Ryan<sup>1</sup> | Charles M. Shobe<sup>1</sup>  | Sara L. Rathburn<sup>2</sup>  | Mark K. Dixon<sup>1</sup>

<sup>1</sup>US Forest Service Rocky Mountain Research Station, Fort Collins, Colorado, USA

<sup>2</sup>Department of Geosciences, Colorado State University, Fort Collins, Colorado, USA

## Correspondence

Charles M. Shobe, US Forest Service Rocky Mountain Research Station, Fort Collins, CO, USA.

Email: [charles.shobe@usda.gov](mailto:charles.shobe@usda.gov)

Sara L. Rathburn, Department of Geosciences, Colorado State University, Fort Collins, CO, USA.

Email: [sara.rathburn@colostate.edu](mailto:sara.rathburn@colostate.edu)

## Funding information

Cities of Fort Collins and Greeley, CO; U.S. Forest Service Rocky Mountain Research Station

## Abstract

Wildfires, and the sediment-rich floods that commonly follow, increasingly threaten riverine ecosystems and water infrastructure. Suspended sediment exported throughout fire–flood sequences poses particular risks due to rapid transit times and direct impacts on water quality. However, opportunities to measure suspended-sediment transport during and after post-fire floods, and therefore to illuminate what controls the magnitude and timing of suspended-sediment export from burned, flooded watersheds, are rare. A ~100-year flood that occurred one year into a three-year study monitoring suspended-sediment response to wildfire in the Colorado Front Range provides a unique opportunity to (1) quantify how suspended-sediment concentrations and loads change throughout a fire–flood sequence, and (2) infer what controls the timescale over which suspended-sediment dynamics recover toward pre-fire conditions. We find that suspended-sediment concentrations (SSCs) during summer storms declined monotonically to background conditions over 3 years. Snowmelt SSCs peaked in the second year before declining to background levels. Sediment load calculations reveal that the flood exported ~35 years' worth of suspended sediment and triggered ~1.5 years of elevated SSCs and sediment loads. SSCs and sediment loads indicate a fairly short post-fire recovery timescale of about 3 years. We suggest that the flood accelerated recovery by (1) exporting much of the available suspended sediment from this supply-limited landscape and (2) facilitating the export of remaining sediment by making it more accessible to subsequent flows. Our results indicate that large post-wildfire floods, though representing major geomorphic disturbances, may hasten post-fire suspended-sediment recovery to background conditions, at least in supply-limited regions.

## KEYWORDS

Colorado Front Range, fluvial geomorphology, post-fire erosion, suspended sediment, watershed disturbance, watershed recovery, wildfire

## 1 | INTRODUCTION

Developing the ability to predict watershed response to disturbances is essential to managing ecosystems and infrastructure (Fryirs, 2017; Phillips & van Dyke, 2016), especially as climate change and human landscape impacts increase disturbance frequency and magnitude

(e.g., Balch et al., 2020). Compound disturbances, in which two or more disturbances interact to influence a landscape (Buma, 2015; Rathburn et al., 2018), are particularly important to understand because of the potential for feedbacks between component disturbances that might drive unexpected landscape response, thereby harming humans and/or the environment.

Fire–flood sequences are an increasingly destructive class of compound disturbances in which a landscape experiences a wildfire followed by a flood event before post-fire recovery is complete. Compound disturbances composed of fires and post-fire floods merit study for both their role as important drivers of landscape change and their importance to land and water management issues (Jong-Levinger et al., 2022). In the American West in particular, warming is driving increased wildfire size, duration, and frequency (e.g., Dennison et al., 2014; Westerling et al., 2006) and also causing increases in thunderstorm precipitation intensity (e.g., Allan & Soden, 2008; Sanderson et al., 2019). Fire strips much of the landscape's protective cover of vegetation, litter, and/or duff, increasing land-surface erodibility (e.g., Larsen et al., 2009; Scott et al., 2009), while increasing runoff generation due to reduced infiltration capacity in burned soils (e.g., Ebel et al., 2012). Major floods, if they occur before complete recovery of soils and vegetation after fire, then exert high erosive stresses across burned landscapes.

Fire–flood sequences combine a disturbance that reduces erosion resistance with one that enhances erosional driving forces. They can therefore drive prolific sediment transport and geomorphic change (e.g., Brogan, MacDonald, et al., 2019; Brogan, Nelson, & MacDonald, 2019; Moody & Martin, 2009; Warrick et al., 2022). Rilling on burned hillslopes can coalesce into, or provide sediment supply for, debris flows in low-order channels (e.g., Alessio et al., 2021; Cannon et al., 2001; McGuire et al., 2017). These flows deliver sediment pulses into mainstem channels (e.g., Brogan, MacDonald, et al., 2019; Brogan, Nelson, & MacDonald, 2019; Rathburn et al., 2018) that, due to flood discharges, high post-fire sediment supply, and fire-induced reductions in bank vegetation, experience rapid changes to channel cross-sectional and longitudinal geometry (Brogan, MacDonald, et al., 2019; Brogan, Nelson, & MacDonald, 2019; Florsheim et al., 2017; Kampf et al., 2016).

Beyond having dramatic geomorphic effects, fire–flood sequences concern scientists and managers because they can produce pulses of rapid bedload and suspended-sediment load export from watersheds (e.g., Malmon et al., 2007; Moody & Martin, 2001). Fire-induced sediment pulses can drive downstream flooding hazards by altering channel conveyance (e.g., Ahrendt et al., 2022) and influence the distribution and quality of aquatic habitat (Goode et al., 2012). They also threaten water quality (Bladon et al., 2014; Martin, 2016) and accelerate reservoir sedimentation (e.g., East et al., 2022; Randle et al., 2021). Combustion products (charcoal, ash, and soot) increase the post-fire suspended-sediment supply, further degrade water quality, and hinder municipal treatment (Chow et al., 2019). The dynamics of suspended-sediment export throughout fire–flood sequences are particularly important because suspended-sediment transit times from burned watersheds to threatened water intakes can be on the order of hours (e.g., Writer et al., 2014). The water-quality and infrastructure effects of post-fire suspended sediment underscore the importance of developing a mechanistic understanding of the controls on suspended-sediment export caused by the compound disturbance of wildfire and post-fire flooding.

Numerous studies assessing post-fire suspended-sediment export (e.g., Dahm et al., 2015; Jumps et al., 2022; Lane et al., 2006; Malmon et al., 2007; Murphy et al., 2015; Oliver et al., 2012; Owens et al., 2013; Petticrew et al., 2006; Reale et al., 2015; Rhoades et al., 2011; Ryan et al., 2011; Silins et al., 2009; Warrick et al., 2012) show highly variable magnitude and duration of suspended-sediment response, both of which seem to depend on post-fire flow sequencing. Malmon et al. (2007) found two-order-of-magnitude increases in SSC at some sites after fire, while Owens et al. (2013) found little fire disturbance of the suspended-sediment regime. In many cases, SSCs in post-fire flow events are greatest immediately after the fire and decline to background (pre-fire) values somewhere between three (Ryan et al., 2011) and seven (Warrick et al., 2012) years post-fire, but a return toward background conditions is not always observed (Rhoades et al., 2011). Variation in watershed response to fire can occur due to differences in geology, climate, vegetation type, the extent of vegetation mortality and consumption, soil burn severity, and land use/management. Past work suggests that the timing, intensity, and sequencing of post-fire precipitation events may be a key control on post-fire sediment dynamics (Brogan, MacDonald, et al., 2019; Brogan, Nelson, & MacDonald, 2019; East et al., 2021; Kampf et al., 2016; Lanini et al., 2009; Murphy et al., 2015; Owens et al., 2013; Warrick et al., 2022; Wilson et al., 2020). The enormous range of natural variability in post-fire catchment hydrology and the inherent rarity of low-recurrence-interval floods make accumulating case studies of fire–flood sequences critical to understanding the processes governing, and hazards associated with, post-fire suspended-sediment export.

Here, we present insights from 3 years of monitoring suspended-sediment dynamics throughout a rare compound disturbance: a severe wildfire followed 15 months later by a ~100-year flood. Our objectives are to (1) quantify how suspended-sediment concentrations (SSCs) and loads change over the course of a fire–flood sequence and subsequent watershed recovery, and (2) elucidate the dominant controls on landscape recovery from these compound disturbances.

## 2 | STUDY AREA DESCRIPTION AND HYDROLOGIC CONTEXT

The South Fork of the Cache la Poudre (SFCLP) is a 272 km<sup>2</sup> watershed that is a major tributary of the Cache la Poudre River, northwest of the City of Fort Collins, Colorado, USA (Figure 1). The watershed lies primarily within the Arapaho–Roosevelt National Forest.

Unburned forest vegetation in the montane zone (1830 to 2740 m) consists of ponderosa pine (*Pinus ponderosa*), lodgepole pine (*Pinus contorta*), and Douglas fir (*Pseudotsuga menziesii*), along with patches of Quaking aspen (*Populus tremuloides*). Open riparian areas contain willow (*Salix* spp.), river birch (*Betula fontinalis*), and aspen and cottonwood (*Populus* spp.). Expected fire severity in the montane zone is variable (Veblen & Donnegan, 2005). In the lower montane, fire may occur as often as every 10 years, while at the upper extent, the fire return interval is likely 100–600 years (Rathburn et al., 2018).

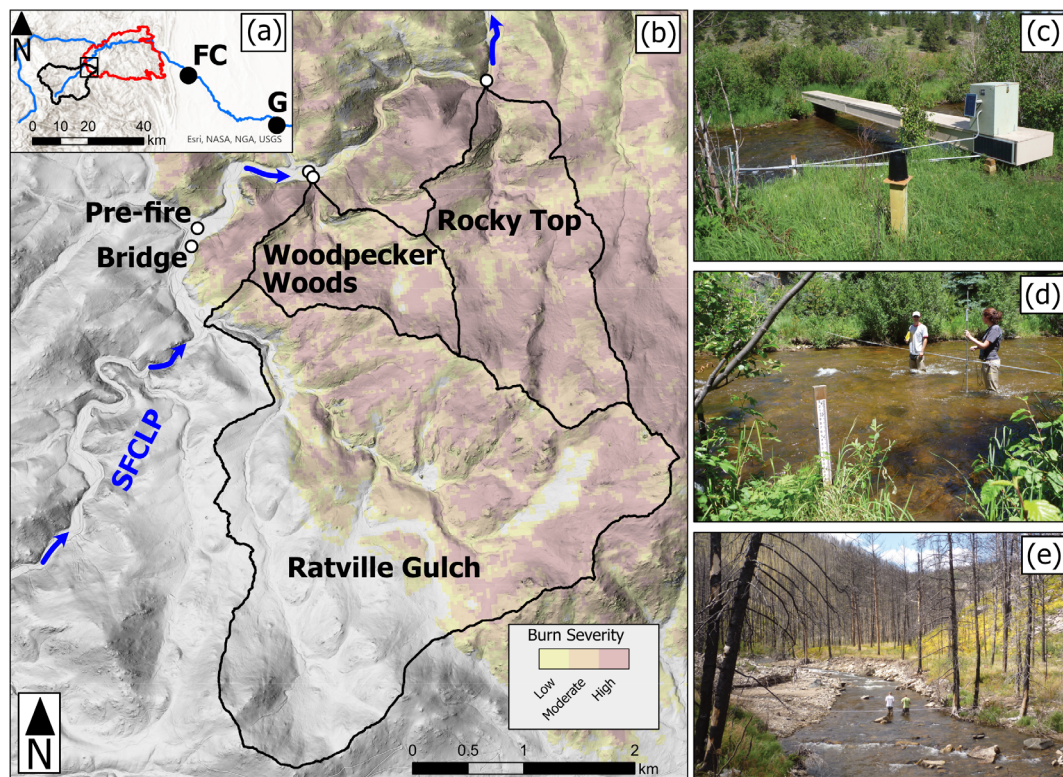


**FIGURE 1** (a) Study area location in the Colorado Front Range. Black box shows extent of (b). 2012 High Park fire perimeter is red, watershed draining to the Bridge site is black, and blue lines show the North Fork, South Fork, and mainstem Cache la Poudre rivers. FC and G are the cities of Fort Collins and Greeley, Colorado, USA, respectively. (b) Lidar-derived multidirectional hillshade with site locations on the SFCLP (dots) and High Park fire burn severity from the Monitoring Trends in Burn Severity project (Eidenshink et al., 2007). Black polygons are watersheds of Ratville Gulch, which is the major source of post-fire sediment to the Bridge site, WPW, and RT. (c–e) Photographs show locations where flow and suspended-sediment data were collected at (a) the Bridge site, (b) SFCLP below the confluence with WPW (view downstream), and (c) the confluence with RT (view upstream) with a fire/flood-derived alluvial fan on left-hand side of the photograph and eroded terrace on the right-hand side. [Color figure can be viewed at [wileyonlinelibrary.com](http://wileyonlinelibrary.com)]

The SFCLP watershed is underlain primarily by granites, gneisses, and schists overlain by glacial debris that represent several glacial advances in the upper portion of the watershed (Green, 1992). Observed channel types (i.e., Montgomery & Buffington, 1997) range from pool-riffle to plane bed, with sections of step-pools and cascades in confined valleys. Precipitation, measured at stations ranging from 2340 to 2390 m in elevation, is primarily snow with short duration, variable-intensity convective storms occurring in summer. Mean annual precipitation is 540 mm (Richer, 2009).

A 23-year (1956–1979) streamgauge record 6 km downstream of our study site (USGS #06748600), with discharge values reduced by 15% to account for the difference in drainage area between the gage and our site, records mean daily discharge ranging from 0.85 to 2.76 m<sup>3</sup> s<sup>-1</sup> in any given year. Annual peak flows range from 5.2 to 30.3 m<sup>3</sup> s<sup>-1</sup>, with an average annual peak flow of 12.9 m<sup>3</sup> s<sup>-1</sup>. Flood frequency calculations using log Pearson III analysis (Interagency Advisory Committee on Water Data, 1982) and the admittedly short peak flow record produce rough estimates for the 2-, 10-, 50-, and 100-year floods of 11.7, 20.9, 29.7, and 33.6 m<sup>3</sup> s<sup>-1</sup>, respectively (Figure 2). The bulk of the annual streamflow in the SFCLP derives from snowmelt that occurs in May, June, and early

July; annual peak flows tend to occur during this period. Summer and early autumn storms drive brief flood events that typically, but not always, have low discharge relative to snowmelt peaks. There are three small dams that store portions of the annual snowmelt that is passed through the SFCLP during late summer months. Releases from these dams can have a substantial impact on baseflows but a negligible effect on SSC during storms and snowmelt (supplemental text S1.1). Outside of occasional storms and dam releases, late summer and early autumn flows tend to remain <5 m<sup>3</sup> s<sup>-1</sup> (Figure 2).

### 3 | THE 2012 HIGH PARK FIRE AND THE 2013 NORTHERN COLORADO FLOOD

The High Park fire burned over 35,000 ha (47% of which burned at moderate or high severity; BAER Team, 2012) largely within the Cache la Poudre basin in Northern Colorado over nearly 1 month during June 2012. Within a week of the fire being contained, moderate-intensity storms generated several debris and hyper-concentrated flows, delivering ash, charcoal, and fine sediment to the Cache la Poudre River and burned tributaries (Kampf et al., 2016; Miller et al.,

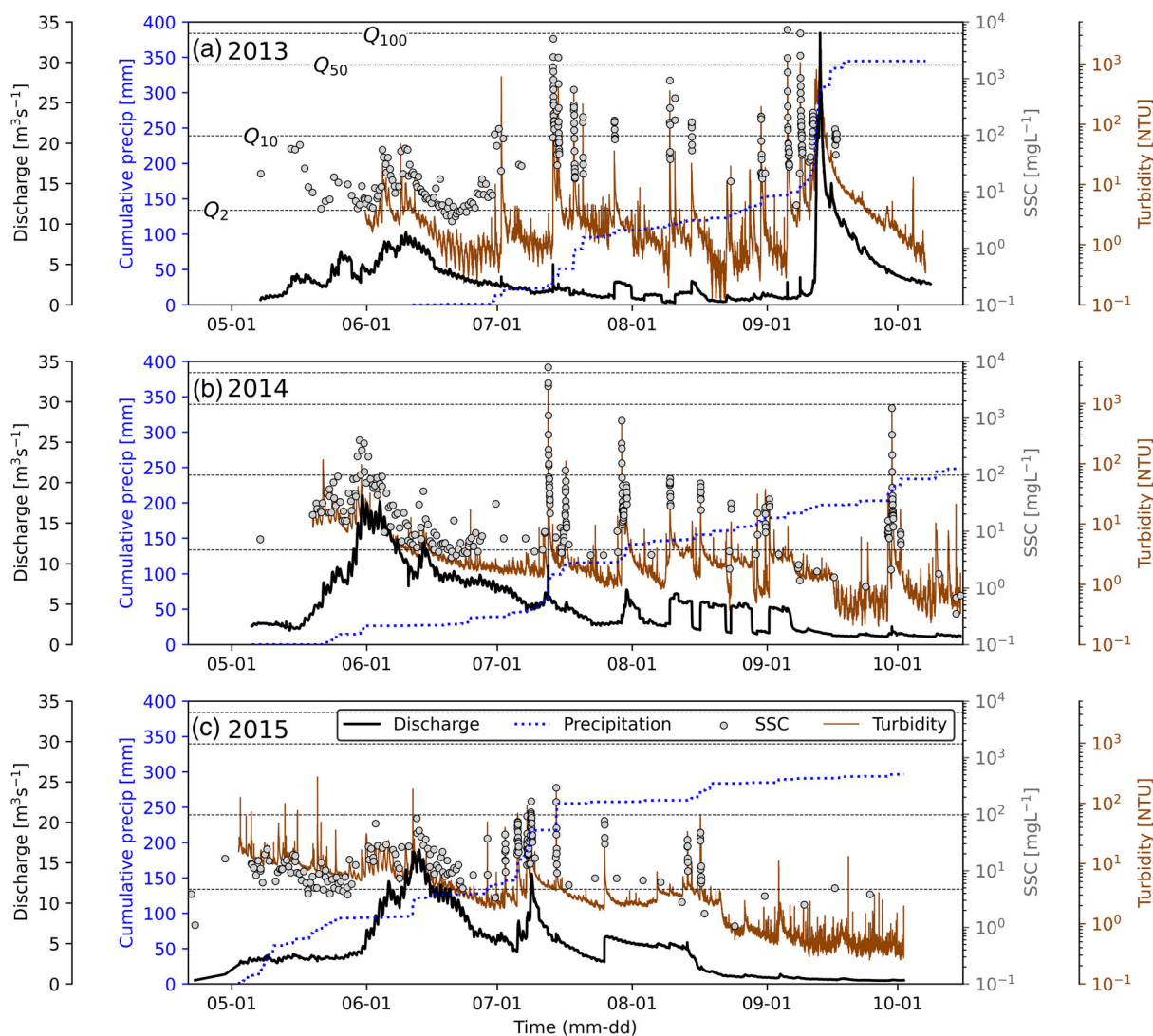


**FIGURE 2** Time series of discharge, cumulative precipitation, SSC, and turbidity for the 3 post-fire years at the Bridge site. Precipitation during the September 2013 flood (09–14 to 09–18) is estimated from a nearby rain gage as ours lost contact with the data logger. [Color figure can be viewed at [wileyonlinelibrary.com](http://wileyonlinelibrary.com)]

2017). Given the proximity of the burn to the water intakes for the cities of Fort Collins and Greeley, Colorado (Figure 1), there was concern over additional sediment delivery to streams over the next several years.

In September 2013, the Colorado Front Range was flooded during a week-long rain event when between 150 and 450 mm of precipitation fell over the mountain front and neighboring plains (Gochis et al., 2015). This event triggered numerous hillslope failures (e.g., Anderson et al., 2015; Patton et al., 2018) and a major flood. In the upper Cache la Poudre River watershed, the amount of rainfall was less than received elsewhere along the Front Range but still substantial (150–200 mm) (Anderson et al., 2015; Gochis et al., 2015). Estimates of the return frequency of the 2013 flood for the Cache la Poudre area are between 25 and 100 years (e.g., Gochis et al., 2015). Our peak discharge estimates from both stage–discharge relationships (supplemental text S1.2) and the critical depth method (supplemental

text S1.3), combined with a 23-year downstream gage record, suggest a recurrence interval of approximately 100 years. While much of the SFCLP study site was disturbed during this event, a pressure transducer and turbidity sensor survived the flood and recorded what appear to be reasonable data, allowing us to estimate flood discharge and suspended-sediment transport.

## 4 | METHODS

### 4.1 | Measurement timing and locations

Our objectives are to quantify suspended-sediment dynamics throughout the fire–flood sequence and subsequent recovery. Some suspended-sediment transport data were collected in the SFCLP prior to the 2012 fire, providing a baseline for comparing to post-fire

sediment loads (Ryan et al., 2005; US Forest Service, unpublished data). Beginning in 2013, we began frequent suspended-sediment data collection during both snowmelt and summer storms. Post-fire measurement methods were comparable to pre-fire methods, but we expanded the types of data collected and number of sites monitored in the post-fire study.

During two pre-fire years (1989 and 1997), 86 total SSC measurements were collected at the site labeled “Pre-fire” in Figure 1. The presence of a beaver dam just upstream of the pre-fire sampling site prevented reoccupation of the exact location in the post-fire years; the “Bridge” study site was established upstream of the tail of the beaver pond (Figure 1). Adjustments of flow estimates were made to compensate for the difference in watershed size between the pre- and post-fire sampling locations. Ratville Gulch, which drains 10.6 km<sup>2</sup> and enters the SFCLP approximately 1 km above the Bridge site (Figure 1), was the primary source of post-fire sediment to the Bridge site as most of the 230 km<sup>2</sup> draining to the Bridge site was unburned (Figure 1a). Greater than 50% of Ratville Gulch burned at moderate or high severity (BAER Team, 2012).

Additional sampling stations were installed at two downstream confluences. The two downstream gulches are referred to as Woodpecker Woods (WPW) and Rocky Top (RT) (Figure 1). Stations were set up above and below the WPW confluence, but only below the RT confluence. Turbidity data were collected at all downstream sites, but SSC was measured only below the confluences. WPW has a contributing area of 1.56 km<sup>2</sup> and ranges from 2390 to 2860 m in elevation. RT encompasses an area of 3.33 km<sup>2</sup> and ranges in elevation from 2340 to 3030 m. Burn severity within the gulches was primarily severe (75%–80% of the area) with most of the remainder of each watershed (~15%) burned at moderate severity (Shahverdian, 2015). Both tributary basins had mulch applied aerially as an erosion-prevention treatment (Figure 1; Rathburn et al., 2018). WPW received straw mulch over a substantial portion of the watershed area, and RT received straw mulch covering a smaller portion of the watershed headwaters.

## 4.2 | Turbidity, suspended-sediment concentration, precipitation, and streamflow measurements

Turbidity was measured primarily using a DTS-12 turbidity probe (Digital Turbidity Sensor, Forest Technology Systems). The DTS-12 has a range of 0–1600 Nephelometric Turbidity Units (NTUs) and a reported accuracy of  $\pm 2\%$  (0–499 NTUs) or 4% (500–1600 NTUs). Stream water samples (for SSC measurements) were collected using an ISCO automated sampler at a fixed point that was approximately half the flow depth. The position was adjusted throughout the season with changes in water level. Samples were collected once every 12 hours during snowmelt runoff. After snowmelt, a turbidity threshold sampling scheme was used to obtain more samples during periods of high turbidity (Lewis & Eads, 2009; Ryan et al., 2006). Once a

turbidity threshold (typically 10 NTUs) was reached, the automated sampler collected samples at 20- or 30-min intervals. Sampling continued until turbidity measurements dropped below the threshold or the 24-position sampler became full. We used our turbidity and SSC data to derive a series of regression models relating the two variables (Rasmussen et al., 2009), enabling continuous estimation of SSCs from the turbidity record. Best-fit regressions varied based on location (Bridge site, WPW, or RT), type of flow event (snowmelt, summer storm, or reservoir release), and suspended-sediment grain size, such that the inferred continuous SSC record at each site is derived from several different relationships, each applied to the appropriate periods of the turbidity record. Regressions were primarily linear or quadratic fits to log-transformed turbidity and SSC values. Detailed methods and specific turbidity–SSC fits are reported in Supplemental text S1.4 and S1.5, Figure S2, and Table S2.

Stage–discharge relationships were developed using standard methods (Nolan & Shields, 2000; supplemental text S1.2). A tipping bucket rain gage with 0.2 mm resolution was located near the Bridge site and recorded data every 10 min. We use peak 30-min rainfall intensity for each storm ( $I_{30}$ ) to identify rainfall thresholds for producing high SSCs. Suspended-sediment loads (SSLs) for snowmelt periods, summer seasons, and the 2013 flood were determined from the sums of daily SSLs. For each sampling interval, the 10-min SSL was determined from the product of turbidity-derived SSC, water discharge, and interval duration. These were summed over the course of each day to determine the daily SSL, which was then summed over the days in each period, season, or storm.

## 4.3 | Statistical methods

A Multi-Response Permutation Procedure (MRPP) was used to determine (1) differences in pre- and post-flood SSCs, (2) between-year differences in post-fire SSCs, and (3) between-site differences in SSCs. MRPP is a nonparametric method for testing for similarity between two or more groups (Cai, 2006; Mielke & Berry, 2007). The MRPP statistic  $\delta_{obs}$  is the mean within-group dissimilarity (Euclidean distance between pairs of observations) averaged over all groups. Small  $\delta_{obs}$  indicates more similarity within groups and vice versa. The null hypothesis is that all groupings of the data are equally probable or in other words that there are no meaningful differences among groups. The data are permuted many times into synthetic groupings to establish the mean within-group dissimilarity  $\delta$  each time the groups are reshuffled. The more permutations for which  $\delta_{obs} \leq \delta$ , indicating that the mean dissimilarity within observed groups is less than the mean dissimilarity within synthetic, permuted groups, the lower the  $p$ -value and the more likely the groups are to be significantly different from one another (Cai, 2006). A sufficiently small  $p$ -value indicates when the null hypothesis of group similarity should be rejected (we use  $p < 0.05$ ). It is important to note that, in an MRPP, significant differences can arise due to differences in group means or in the spread of measurements.

## 5 | RESULTS

### 5.1 | Precipitation and streamflow

Precipitation and streamflow differed among the three post-fire years (Figure 2). The first year, 2013, had a relatively low snowmelt peak and frequent low- to moderate-intensity rainfall in the summer, followed by the exceptional 2013 flood. The snowmelt peak was  $8.8 \text{ m}^3 \text{ s}^{-1}$  or about 90% of the channelized flow. There were 15 events in 2013 that produced rises in turbidity that triggered the automated sampler at the Bridge site. Most of these were rainstorms, although three were associated with rapid increases in discharge following reservoir releases. Peak 30-min rainfall intensity for the sampled storms ranged from  $3.2$  to  $30 \text{ mm hr}^{-1}$ . The latter storm has a return frequency of once in  $\sim 2$  years (Table S1 gives reported  $I_{30}$  recurrence intervals).

The 2013 flood in the SFCLP basin was immediately preceded by two low-intensity rainstorms. A significant rise in the hydrograph began late on 11 September (Figure 3). At 12:40 on 12 September, the pressure transducer at the Bridge site was dislodged by the high flows. A second pressure transducer located downstream (just above the confluence with WPW) remained intact, permitting reconstruction of the flood hydrograph and estimation of peak flood discharges for the Bridge site. The estimated peak flow, based on extrapolation of the rating curve, was  $33.6 \text{ m}^3 \text{ s}^{-1}$  or about 3.5x the channelized discharge. The critical depth method reveals an inferred peak flow of  $37.7 \text{ m}^3 \text{ s}^{-1}$  (see Supplemental text S1.3). While both methods are subject to error, they establish a range of peak flood flows. On 14 September, the datalogger lost contact with the rain gage. Based on values from nearby rain gages, an estimated 23 mm of rain fell in the area on 15 September, causing a final hydrograph peak ( $14.7 \text{ m}^3 \text{ s}^{-1}$ ). Flow recession was gradual; the water level was still close to the tops of the banks during a site visit on 17 September. Estimated discharge during that visit was  $10.2 \text{ m}^3 \text{ s}^{-1}$ , based on the

standing staff plate and extrapolation of the rating curve. Flows were still considerably above pre-flood baseflow in late autumn after data collection ended for the season.

In 2014, there was an extended snowmelt peak (2 weeks out-of-bank), with one short, high-intensity storm and several longer-duration storms of note. The snowmelt peak was estimated at  $18.1 \text{ m}^3 \text{ s}^{-1}$  or approximately 1.8x the channelized flow. 2014 saw eight storms that triggered the automated sampler. Peak 30-min rainfall intensity for the sampled storms ranged from  $3.2$  to  $49 \text{ mm hr}^{-1}$ , the latter of which has an estimated return frequency of nearly 10 years (Table S1) and had the highest intensity rainfall of any storm during the study.

The 2015 runoff year also had an extended—though later occurring—snowmelt peak followed by a few low- to moderate-intensity storms. Peak discharge was  $16.4 \text{ m}^3 \text{ s}^{-1}$ , which was 1.7x the channelized discharge. In 2015, there were nine events that triggered the automated sampler. Peak 30-min rainfall intensity for the sampled storms ranged from  $11$  to  $36.8 \text{ mm hr}^{-1}$ —about a 3-year return frequency (Table S1).

The estimated flow return frequencies for the snowmelt peak flows for the 3 years were 1.5, 5–8, and 5 years, respectively, indicating that 2014 had the greatest snowmelt discharge. An MRPP analysis on all storms with  $I_{30} > 10 \text{ mm hr}^{-1}$  indicates that summer storm rainfall intensities were not significantly different among the 3 years ( $p = 0.32$ ), although there were fewer such storms in 2015 (5) than in 2013 (7) and 2014 (7).

### 5.2 | Suspended-sediment concentrations over time

SSCs measured prior to the 2012 fire were typically  $< 50 \text{ mg L}^{-1}$ , with a few samples  $> 100 \text{ mg L}^{-1}$  (Figure 4, striped box). This range is comparable to other measurements from small, undisturbed streams

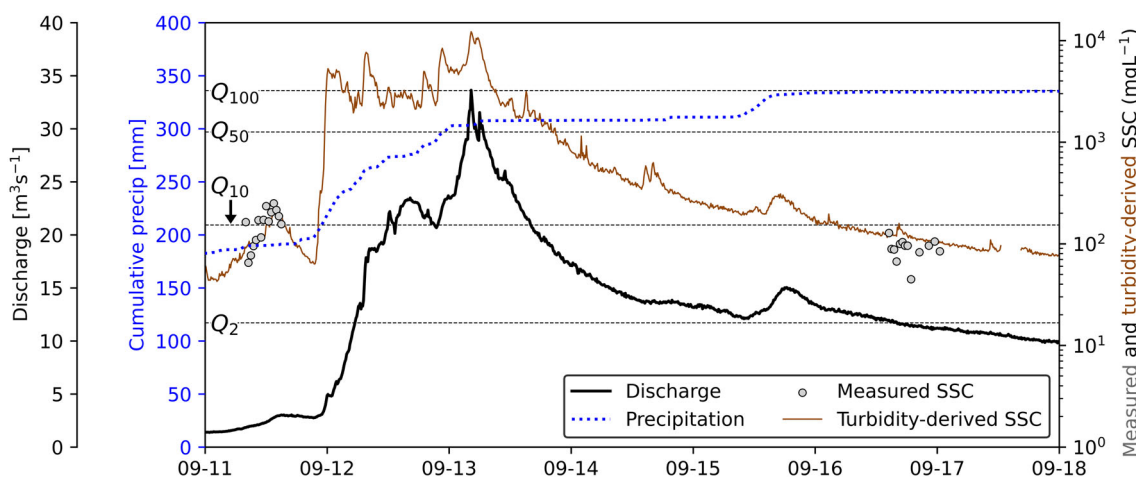
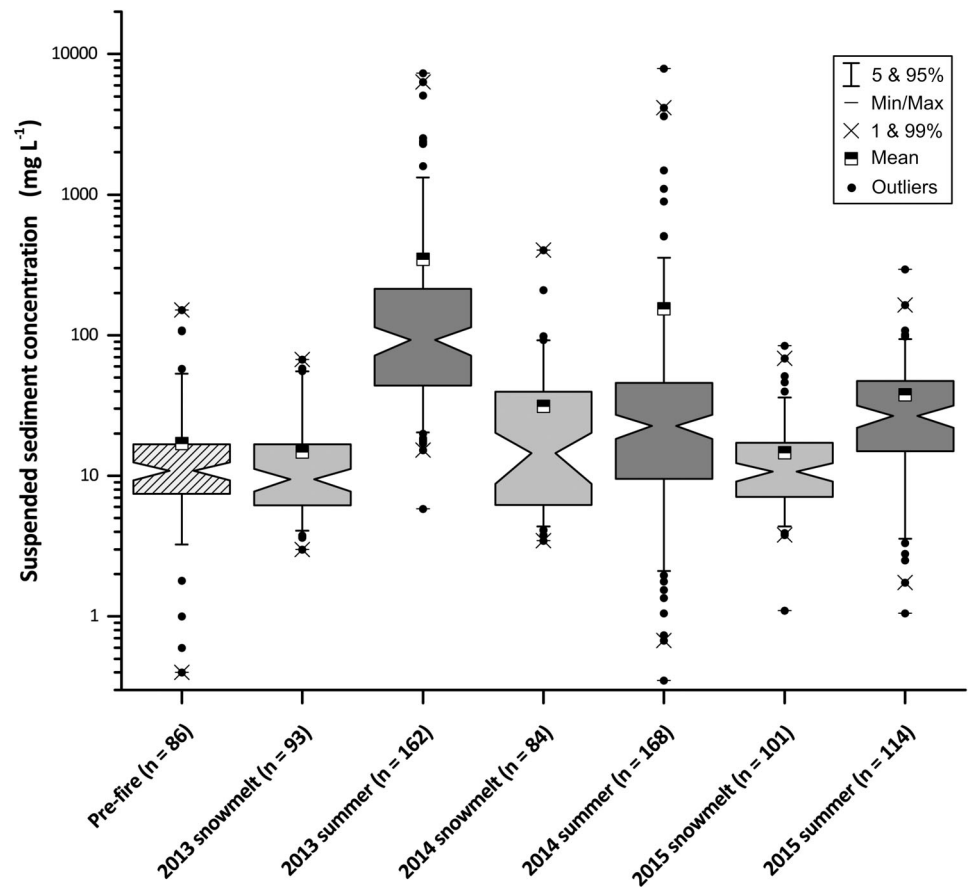


**FIGURE 3** Time series of discharge, precipitation, turbidity, and SSC at the Bridge site during the September 2013 flood. Discharge is estimated from a composite pressure transducer record (Section 5.1) as the transducer at the Bridge site was dislodged by the flood on 12 September at 12:40. Precipitation from 09–14 to 09–18 is estimated from a nearby rain gage as the Bridge site rain gage lost contact with the data logger during this time. Falling-limb SSC measurements come from the WPW sampler as the Bridge site sampler was damaged by the flood. [Color figure can be viewed at [wileyonlinelibrary.com](http://wileyonlinelibrary.com)]

**FIGURE 4** Measured SSCs at Bridge site for pre-fire years (striped), post-fire snowmelt (light gray), and summer storm periods (dark gray). Notches show confidence interval around the median. Box edges are the 25th and 75th percentiles. 2013 summer includes the 2013 flood period, but there are no measured SSCs from near-peak flows during that event (Figure 3).



draining the crystalline bedrock of the Colorado Front Range (e.g., Andrews, 1984; Elliott, 1988). Pre-fire samples were collected primarily during snowmelt runoff because previous collection efforts focused on processes occurring during the annual freshet (Supplemental text S1.6). While it is fortunate that we have any pre-fire SSC data at all, the lack of pre-fire samples from summer storms does present a limitation when comparing to post-fire SSCs.

Data from 2013, the first post-fire year we monitored, show both similarities to (during snowmelt) and departures from (during summer storms) pre-fire values. Snowmelt data from 2013 fall largely within the same range as the pre-fire data (Figure 4). An MRPP comparing pre-fire data (up to a discharge of  $7 \text{ m}^3 \text{ s}^{-1}$  for consistency with 2013's low snowmelt discharges) and first year post-fire snowmelt data indicates differences are not significant ( $p = 0.41$ ). In contrast, SSC samples collected during the summer 2013 storms that predate the September 2013 flood are up to 2 orders of magnitude greater than comparable baseline flows, a statistically significant difference.

Though no SSC samples were collected during the 2013 flood, the Bridge site turbidity sensor survived and recorded what appear to be reasonable data during the sustained high flows. Turbidity ranged from 500 NTUs at the onset of the flood to 1260 NTUs near peak runoff (Figure 3). These values are within the reported sensor range. We used SSC samples from reservoir release flows as well as those collected during a storm on September 11, 2013—just prior to the onset of the flood—to infer SSC values during the

flood from measured turbidity (see “High sand events (pre 2013 flood)” calibration in Table S2 and the dashed line in Figure S2A). These flows were used to calibrate the turbidity–SSC relation for the 2013 flood because we expect their high SSCs and sand content to be most representative of flood conditions. Turbidity-derived flood SSC estimates ranged from 2000 to  $12,000 \text{ mg L}^{-1}$ . We suspect that these peak estimates are low due to exceptionally high sand transport in suspension during the flood that may not be captured by turbidity measurements. However, we were able to use the turbidity–SSC relationship to predict, with only minor over-estimation, the concentrations of samples collected by the WPW sampler during the falling limb of the flood (Figure 3). Maximum SSC during the flood was coincident with a rapid hydrograph rise to the peak discharge. Thereafter, concentrations declined as flow receded, reaching  $100 \text{ mg L}^{-1}$  on 17 September and less than  $10 \text{ mg L}^{-1}$  on 3 October.

SSCs for 2014 snowmelt are significantly greater and show greater variability compared to pre-fire values (Figure 4). Because there were few samples collected at low discharge measurements during 2014 snowmelt, the pre-fire data were truncated to the range of common discharge ( $5\text{--}15 \text{ m}^3 \text{ s}^{-1}$ ) for comparison. 2014 snowmelt SSCs are significantly greater than pre-fire SSCs ( $p < 0.01$ ). Comparison of SSCs from 2014 summer storms with those from 2013 summer storms indicates that 2014 values were significantly lower than 2013 values ( $p < 0.001$ ).

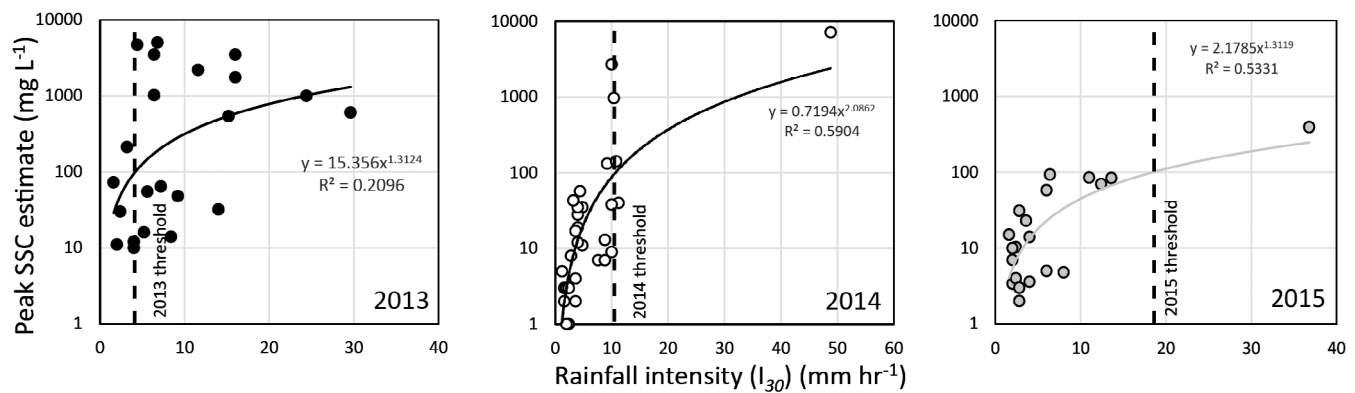


**FIGURE 5** Relationships between rainfall intensity and peak SSC for post-fire summer storms at the Bridge site by year. Vertical lines mark the intensity needed to generate SSCs of over  $100 \text{ mg L}^{-1}$ , the measured upper limit for pre-fire SSCs. Increasingly intense rainfall was needed to generate SSCs above this threshold as time elapsed since the fire.

In 2015, measured concentrations during snowmelt runoff were lower than 2014 snowmelt values and were statistically identical to pre-fire and 2013 values (Figure 4). Results of the MRPP for the summer storms indicate significant differences between 2014 and 2015 ( $p = 0.015$ ). Samples collected during the summer 2015 storms lack the high concentrations observed in 2014 summer storms; the largest measured SSC in 2015 was about  $300 \text{ mg L}^{-1}$ . The general pattern we observe is that for the snowmelt season, SSCs increased in 2014 and decreased again in 2015. During the summer storm season, mean SSCs declined year over year.

As time elapsed post-fire, progressively more intense rainfall was required to generate SSCs above  $100 \text{ mg L}^{-1}$ , an approximate upper limit for pre-fire SSCs (Figure 4). Plotting rainfall intensities ( $I_{30}$ ) against estimated peak SSCs for all storms each year (Figure 5), 2013 shows a weak relationship between  $I_{30}$  and peak SSC because small storms ( $I_{30} < 10 \text{ mm hr}^{-1}$ ) generated a wide range of SSCs, including several values  $> 1000 \text{ mg L}^{-1}$ . Over a third of 2013 storms where  $I_{30}$  was  $< 10 \text{ mm hr}^{-1}$  produced peak SSCs greater than  $100 \text{ mg L}^{-1}$  and nearly all storms with  $I_{30} > 10 \text{ mm hr}^{-1}$  generated SSCs  $> 100 \text{ mg L}^{-1}$  (Figure 5). Fitting a power law to the 2013  $I_{30}$ -SSC relationship indicates that the threshold  $I_{30}$  for exceeding  $100 \text{ mg L}^{-1}$  is approximately  $4 \text{ mm hr}^{-1}$ , although the prevalence of high SSCs even for low-intensity rainstorms causes the fit to be poor. In 2014, lower-intensity storms produced peak SSCs of  $10$ – $100 \text{ mg L}^{-1}$  but did not, in general, produce peak SSCs  $> 100 \text{ mg L}^{-1}$ . Most 2014 storms with  $I_{30} > 10 \text{ mm hr}^{-1}$  generated peak SSCs  $> 100 \text{ mg L}^{-1}$ . 2014 experienced an  $I_{30}$  threshold required to generate SSCs  $> 100 \text{ mg L}^{-1}$  of  $10 \text{ mm hr}^{-1}$ , much greater than 2013's threshold of  $4 \text{ mm hr}^{-1}$  (Figure 5). By 2015, this rainfall intensity threshold shifted to almost  $20 \text{ mm hr}^{-1}$ , with only one storm producing peak SSCs  $> 100 \text{ mg L}^{-1}$  (Figure 5). The power-law fits defining the 2014 and 2015 thresholds are much better than for 2013 due to a lack of high SSC values for low-intensity storms in the two latter years. In general, the rainfall intensity required to produce SSCs  $> 100 \text{ mg L}^{-1}$  increased with time since the fire.

Storm-by-storm SSCs estimated from turbidity-SSC regressions indicate that, on average, SSCs declined with time post-fire at all three

sites and that SSCs were much lower after the 2013 flood than before (Figure 6). Maximum SSCs during 2013 storms routinely exceeded  $1000 \text{ mg L}^{-1}$  and even relatively low-intensity storms (e.g., the 5 September 2013 storm) generated SSCs  $> 1000 \text{ mg L}^{-1}$ . SSCs declined during storms after the 2013 flood, apart from the first storm of 2014. SSC values only exceeded  $1000 \text{ mg L}^{-1}$  during three storms in 2014. 2014 also saw the first storms in which concentrations remained below  $100 \text{ mg L}^{-1}$  at some sites. Only one storm in 2015 (July 14, 2015) produced SSCs greater than  $100 \text{ mg L}^{-1}$ .

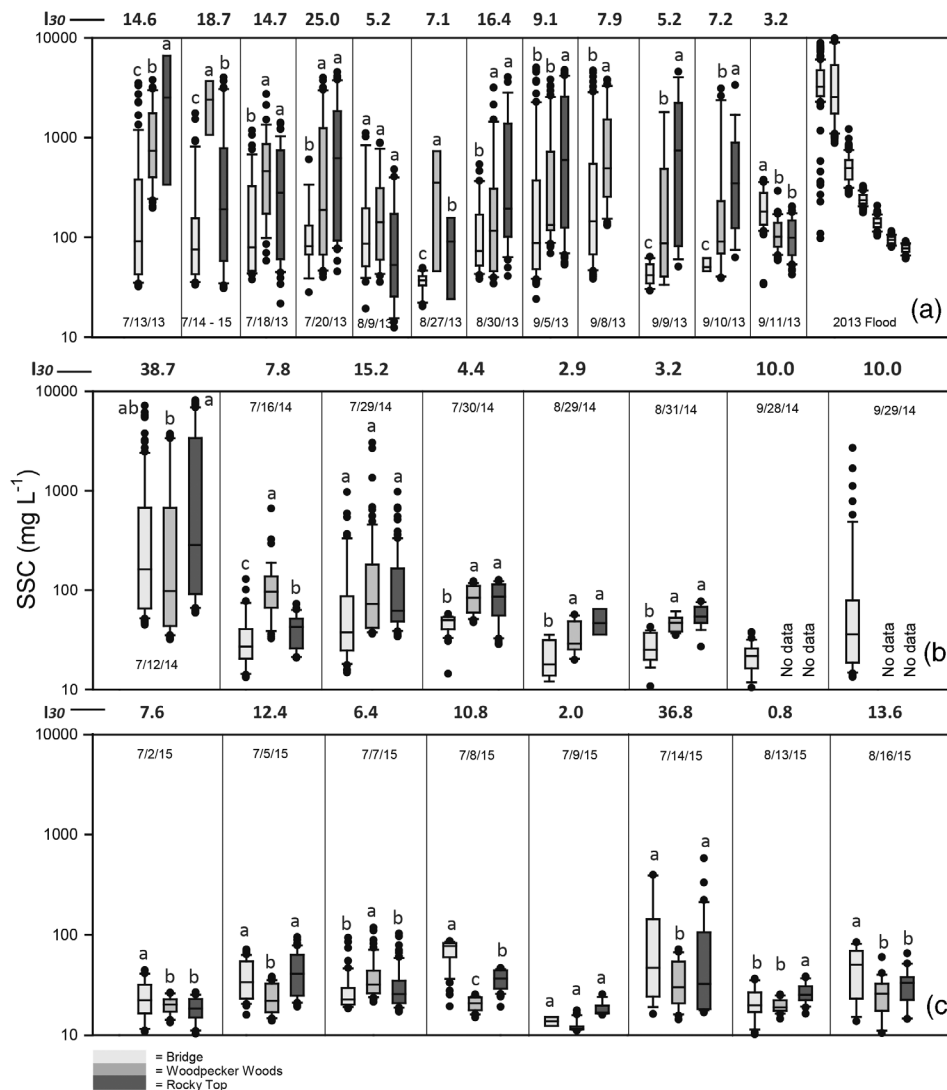
Differences in SSCs between the two tributary sites, which had 75%–80% of their area severely burned, and the Bridge site, which drains a much greater area that was largely unburned, also decline with time post-fire. The tributary sites had higher SSCs than the Bridge site for most 2013 storms (Figure 6a). No tributary had consistently higher SSCs than the other. By 2014, the differences in estimated SSC between the tributaries and the Bridge site were decreasing in absolute terms but were significant for most storms for which we have data (Figure 6b). The two largest storms (12 and 29–30 July 2014) show comparable concentrations at all three sites. The similarity in SSCs among the three sites continued through 2015 as concentrations declined at all sites (Figure 6c). While there were some statistically significant differences among sites in 2015, the absolute differences between sites were quite small ( $\sim 20 \text{ mg L}^{-1}$ ). Storm-by-storm results indicate that differences among sites declined alongside declines in SSCs at all sites both over time since fire and after the 2013 flood relative to before.

### 5.3 | Sediment loads over time

Pre-fire SSLs from the SFCLP are uncertain, but a rough estimate of annual load can be made using the pre-fire SSC measurements from 1989 and 1997 and the flow record from the USGS gage downstream of the study site that existed between 1956 and 1979. Based on this accounting, mean annual SSLs are on the order of  $460 \text{ t}$  (Figure 7, dashed line), ranging from  $170$  to  $1200 \text{ t}$  in low to high years,



**FIGURE 6** SSCs inferred from turbidity–SSC regressions at the three sites for individual storms in (a) 2013, (b) 2014, and (c) 2015.  $I_{30}$  from the Bridge site rain gage is in bold above the plots. Lowercase letters indicate statistical (dis)similarity among sites, with common letters indicating sites with similar SSCs. The a-values had highest median values, c-values were lowest, and b-values were intermediate. “No data” values in (b) exist because the stations had been dismantled for the year.



respectively. These values are within the range calculated using data for Colorado streams with similar geology and land use (Elliott, 1988; Elliott & DeFeyter, 1986). Historically, most of the sediment transport occurs during the snowmelt period from May to June in most years and there is little contribution from summer storms in undisturbed watersheds.

Annual SSLs for the post-fire years exceeded the estimated mean annual load (Figure 7). 2013 snowmelt runoff was relatively low (Figure 2) and had SSCs comparable to pre-fire values (Figure 4), producing a low load (<300 t; Figure 7). Snowmelt and summer flows contributed to the annual load almost equally until the 2013 flood, suggesting that the effect of the fire was a modest increase in the annual sediment load for that year relative to the pre-fire annual load (Figure 7). The very high 2013 annual load was a result of the exceptional flood, which we loosely estimate to have transported an additional 16,000 t of suspended sediment (Figure 7). Although there is considerable uncertainty associated with this value (Supplemental text S1.3), it far exceeds loads calculated for any other period for which we have more certainty (max of ~3000 t). The pre-flood

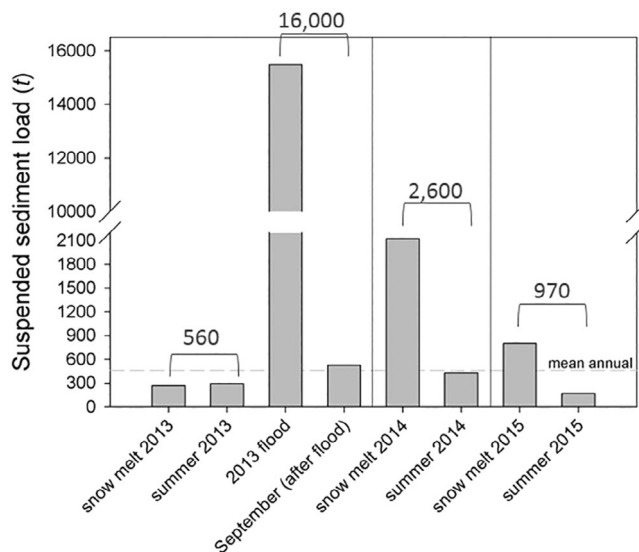


**FIGURE 7** Estimated sediment loads for the 3 post-fire years. Numbers above bars indicate total for each time interval.

summer storms of 2013 contributed to a total annual pre-flood load only slightly greater than background (Figure 7). By contrast, the September 2013 flood appears to have exported approximately 35 years' worth of suspended sediment.

Snowmelt in 2014 was 1.8x the channelized discharge and remained out-of-bank for more than 2 weeks (Figure 2). Measured SSCs for snowmelt were higher than in other years (Figure 4). As a result of both high flow and high sediment concentrations, the estimated sediment load for the 2014 snowmelt period is the highest of the 3 years (2100 t; Figure 7). The load estimated for the summer storms in 2014 (430 t) is greater than that estimated for the pre-flood summer 2013 storms (300 t), even though 2014 summer storm SSCs were somewhat lower than in 2013 (Figure 4). This is due to higher baseflow in 2014 (Figure 2), likely from the lingering effects of saturated post-flood conditions combined with high snowpack. Snowmelt runoff was high again in 2015 (1.7x the channelized discharge) and lasted for over 2 weeks. Measured SSCs were comparable to pre-fire estimates (Figure 4) and so the load estimates for the snowmelt period are likely analogous to pre-fire values in a high-runoff year (800 t; Figure 7). Total SSL for 2015 summer storms was the lowest of any period measured.

## 6 | DISCUSSION

The type of compound disturbance fortuitously captured in this study, a severe fire closely followed by a  $\sim 100$ -year flood, is expected to become more common as climate change increases aridity and storm intensity across the western United States and elsewhere. Using our detailed dataset to infer what controls the magnitude and timing of post-fire suspended-sediment export can both illuminate how watersheds respond to fire-flood sequences and inform future management approaches to protecting aquatic ecosystems, water quality, and infrastructure.

### 6.1 | Suspended-sediment concentrations, loads, and post-fire recovery

By 2015, or about 2.5–3 years post-fire, SSCs largely returned to pre-fire levels from peaks nearly two (snowmelt; highest SSCs observed in 2014) and almost three (summer storms; highest SSCs observed in 2013) orders of magnitude above pre-fire levels, with the caveat that pre-fire values largely represent snowmelt rather than summer storms (Figures 4–6). No SSCs  $>1000 \text{ mg L}^{-1}$  were observed in 2015, indicating that such high SSCs could not be generated despite the study area experiencing rainfall events that year that would have generated SSCs  $>1000 \text{ mg L}^{-1}$  in 2013 and 2014. Although there were fewer storms with  $I_{30} >10 \text{ mm hr}^{-1}$  in 2014 and 2015 than there were in 2013, relationships between  $I_{30}$  and SSCs show that increasingly intense rainfall was required to generate a given SSC as time elapsed (Figure 5), providing further evidence for a rapid decline in the importance of fire effects on the suspended-sediment signal. Our

observations from the mainstem SFCLP are consistent with temporal patterns in intensity–SSC relationships observed at the outlets of the WPW and RT tributaries, in which increasingly high  $I_{30}$  was required to produce SSC values above  $100 \text{ mg L}^{-1}$  as time elapsed since the fire (Rathburn et al., 2018, their Figure 5).

Summer storms generated higher peak SSCs than did snowmelt runoff (Figure 4), but snowmelt dominated annual sediment loads in our study area (Figure 7). This occurs because summer storm discharges arise from short-lived, convective thunderstorms and, excepting the 2013 flood, do not generate discharges as high, or flow durations as long, as those observed during snowmelt runoff (Figure 2). Our data support the idea that summer storms are more likely than snowmelt runoff to initially have dramatically increased SSCs due to fire and are therefore more likely to demonstrate clear post-fire declines in SSC over time. The exceptional SSCs of summer storms mean that they may be a more important focus for managers than are snowmelt runoff events, which carry much lower SSCs. Aside from rare summer floods, however, evacuation of suspended sediment is predominantly a snowmelt runoff-driven process both in our study region in general and after fire in particular. The dominance of snowmelt runoff as a driver of post-fire sediment export sets our study area apart from commonly studied regions like southern California (e.g., Florsheim et al., 2017; Keller et al., 1997; Rengers et al., 2021), which has many fires and post-fire storms but no snowmelt contribution to post-fire sediment dynamics.

Our results are broadly consistent with the expectation that the first storms measured post-fire should generate the highest SSCs and that SSCs and sediment loads should generally decline over time since the fire (Guilinger et al., 2020; Ryan et al., 2011; Warrick et al., 2012). We identify a recovery timescale for the suspended-sediment regime in our study area of approximately 3 years, based on SSCs (Figures 4 and 6), rainfall intensity–SSC relationships (Figure 5), and sediment loads (Figure 7). If 2015 SSCs and sediment loads do mark the permanent return of loads to pre-fire levels (of this we cannot be certain given that monitoring ended after 2015), the 3-year recovery of suspended-sediment dynamics in our study area to background conditions would be on the short end relative to other studies (e.g., Warrick et al., 2012), including some in the Colorado Front Range (Rhoades et al., 2011). We emphasize that the return of SSCs and loads to background conditions does not imply full recovery of the watershed from the fire; other work in our study area and elsewhere shows that morphologic adjustment of channels continues even after suspended-sediment export stabilizes (e.g., Owens et al., 2013; Rathburn et al., 2018; Ryan et al., 2011; Wohl et al., 2023). Nevertheless, the suspended-sediment recovery we observe is rapid.

The observed declines in summer storm SSCs and increases in  $I_{30}$  required to generate SSCs exceeding pre-fire values could be due to either soil stabilization by returning vegetation or a supply limitation on sediments able to be transported in suspension. While we do not have direct evidence allowing us to quantify the relative impact of vegetation stabilization versus sediment supply limitations as mechanisms for SSC reductions over time, we suggest that both play a role. Field measurements indicate that regrowth of vegetation after the fire

and flood increased ground cover from 28% to 47% at the WPW site, and from 30% to 57% at the RT site, between July 2013 and July 2014 (Rathburn et al., 2018, their tab. 2). Remote sensing also indicates vegetation regrowth; the Normalized Difference Vegetation Index (NDVI) of the moderately and severely burned portions of the High Park burn area increased between 2013 and 2015 (A. Vorster and M. Innes, personal communication, 2024). Some amount of vegetation stabilization is therefore probable. However, the abundance of bare, and probably therefore very erodible, soil in 2014 (Rathburn et al., 2018) and the fact that 2015 NDVI values are low relative to pre-fire values (A. Vorster and M. Innes, personal communication, 2024) suggest that revegetation cannot have fully stabilized the soil by that point. We therefore hypothesize that sediment supply limitations also play a role in reducing SSCs and sediment loads over time. Supply-limited sediment dynamics have been inferred in burned areas across the Colorado Front Range (Moody et al., 2008; Morris & Moses, 1987; Wohl et al., 2023) and may result from the low soil depths in the region (e.g., Diek et al., 2014). Supply limitations could arise due to progressively declining soil erodibility as the most erodible materials are stripped away in the earliest storms (Kampf et al., 2016) or simply due to declining abundance of suspension-sized sediment.

While summer SSCs and sediment loads exhibit the expected monotonic decline over time since fire, snowmelt SSCs and sediment loads do not. We observe low SSCs (Figure 4) and sediment loads (Figure 7) during spring 2013 snowmelt relative to the higher concentrations and loads observed during the spring 2014 snowmelt season. We cannot rule out that the difference in snowmelt sediment loads from 2013 to 2014 can be mostly explained by the factor-of-two increase in peak snowmelt discharge between 2013 and 2014. However, we suggest another, intrinsic control rooted in sediment supply limitations that may help explain (1) the short recovery timescale of the suspended-sediment regime in our study area, (2) the higher SSCs observed during 2014 snowmelt relative to 2013, and (3) the nearly order-of-magnitude increase in 2014 snowmelt sediment loads over 2013.

## 6.2 | The influence of a major flood early in post-fire recovery

We attribute both the relatively short response time and the complex temporal patterns in snowmelt SSC and sediment load to the 2013 flood exporting—or preparing for export—the bulk of the post-fire suspended-sediment supply, leaving the study area in a supply-limited state. We hypothesize that the flood, in addition to exporting ~35 years' worth of sediment during the event itself, increased the erodibility of sediment left behind in the study catchments by detaching fine sediment and depositing it where it could easily be accessed by subsequent flows (e.g., in channels; Salant et al., 2007). The increased SSCs during 2014 snowmelt, and the consequent yield of several years' worth of suspended sediment during that period, may have been partially enabled by re-entrainment of sediment that was

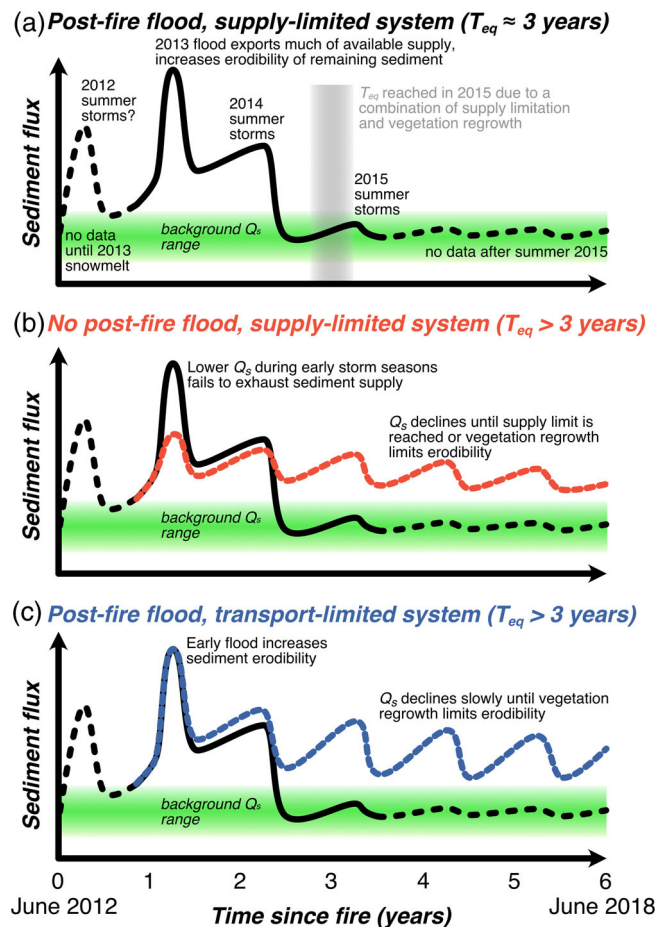


**FIGURE 8** (a) Conceptual model of suspended-sediment recovery in our study area, inspired by Keller et al. (1997; their Figures 8 and 9) and Rathburn et al. (2018; their Figure 8). Sediment flux ( $Q_s$ ) time series (black line) from (a) is repeated in (b) and (c) to facilitate comparison. Green region indicates background (pre-disturbance) range of sediment fluxes. We interpret our inferred ~3-year recovery timescale,  $T_{eq}$ , to result from a combination of a major post-fire flood and sediment supply limitations, in addition to post-fire vegetation regrowth. (b) In the absence of a post-fire flood, we might expect a longer  $T_{eq}$ , even if sediment supply is limited. (c) Transport-limited conditions, even if a flood occurs, may slow suspended-sediment recovery. [Color figure can be viewed at [wileyonlinelibrary.com](https://onlinelibrary.wiley.com/terms-and-conditions)]

initially mobilized during the 2013 flood. The occurrence of a major flood so soon after a severe wildfire may have therefore acted as an accelerant to recovery of the system toward background suspended-sediment conditions (Figure 8). Although lidar differencing and grain size measurements in small drainages near our study area show that the 2013 flood was predominantly erosive (Brogan, MacDonald, et al., 2019; Brogan, Nelson, & MacDonald, 2019), the flood did cause up to a meter of in-channel deposition at some points along the channel network, especially in downstream reaches (Brogan, MacDonald, et al., 2019; Brogan, Nelson, & MacDonald, 2019; Kampf et al., 2016). Similar flood-driven deposition in our much larger study stream could provide an easily accessible source of post-flood suspended sediment, thereby accelerating post-fire recovery of the suspended-sediment regime.

### 6.3 | Conceptualizing suspended-sediment response to fire–flood sequences

Post-fire suspended-sediment monitoring studies are motivated by the questions “How much?” and “For how long?”, the goal being to develop predictive power over (1) the peak SSCs and loads expected in streams and (2) the length of time that recovery to background conditions will take. We find evidence that the 2013 flood influenced both event-scale sediment export and the trajectory of post-fire suspended-sediment recovery. Generalizing from our results provides an opportunity to assess how recovery from the fire would have been different had the study area experienced different hydrologic forcing during the first three post-fire years, as well as to develop a conceptual model for what controls the recovery process in burned landscapes more generally.

The 2013 flood appears to have had a strong effect on peak SSCs and loads over the study period. It produced the highest single-storm SSCs we observed (Figure 6) and yielded approximately 35 years' worth of suspended sediment (Figure 7) due to its high SSCs, high water discharge, and long duration. In only ~1 month after the flood, the SFCLP exported more than a years' worth of suspended sediment (Figure 7). The following (2014) snowmelt season yielded the highest sediment loads in the study aside from the 2013 flood, representing several years' worth of suspended sediment. We infer from these prolific post-flood SSLs that receding floodwaters left significant amounts of sediment in an easily erodible state. This suggests that major flood events coming soon after severe fire may generate not just one but a sequence of transport events with elevated SSCs and sediment loads (Figure 8).

Because a major flood occurring soon after a severe fire accelerates suspended-sediment export, it also likely influences the timescale over which SSCs and sediment loads return to pre-fire levels (Figure 8a versus b). In a supply-limited landscape, efficient export of suspended sediment by a major flood and subsequent high flows that re-entrain flood-derived sediment (Figure 8a) means that the supply limit is reached, and sediment fluxes return to their pre-disturbance range of variability (green shaded region of Figure 8), sooner than if a major flood had not occurred (Figure 8b). We infer that, after suspended sediment made more erodible by the flood had been exported, sediment supply joined vegetation-driven soil stabilization as a limiter of suspended-sediment transport.

In the opposite end-member case of transport rather than supply limitation, as might be experienced in a landscape with thicker soils, a major suspended-sediment-flushing event like the 2013 flood may not meaningfully reduce—and could even increase—the watershed recovery timescale until vegetation regrowth stabilizes the soil (Figure 8c). Major post-fire floods in transport-limited landscapes might represent an additional disturbance to the suspended-sediment regime rather than a force that accelerates the return of the suspended-sediment signal to pre-fire conditions (Figure 8c) as we interpret occurred at our sites. In transport-limited cases, erodibility reduction due to soil stabilization by vegetation regrowth would be the process by which suspended-sediment export returns to

background conditions. Because thick soils tend to occur in regions with rapid vegetation regrowth rates, regrowth may commonly be rapid enough that the potential erodibility-increasing effects of a post-fire flood (Figure 8c) do not meaningfully change the suspended-sediment response to fire–flood sequences in transport-limited landscapes. Semi-arid landscapes, which have sufficient vegetation to sustain a fire but slow vegetation regrowth rates, may be the most susceptible to long-lived disturbances to the sediment regime driven by fire–flood sequences (Goode et al., 2012; Sankey et al., 2017).

The recovery timescale  $T_{eq}$  for landscapes with meaningful supply limitations (i.e., those in which recovery is driven by exhaustion of a supply of erodible post-fire sediment) can be thought of as the residence time of suspension-sized sediment within a burned watershed; it approximates the (in)ability of a watershed to recover from a fire by exporting the available supply of suspended sediment.  $T_{eq}$  [T] can be conceptualized as a function of post-fire suspended-sediment supply volume  $V$  [ $L^3$ ] available in the landscape, the water discharge of any post-fire flood(s)  $Q_w$  [ $L^3T^{-1}$ ], which serves as a proxy for the erosive stresses imposed on the land surface, and the average concentration of sediment across any flood events that occur  $C_s$  [ $L^3L^{-3}$ ] ( $C_s$  could alternatively have units of mass per volume if  $C_s$  was then divided by sediment grain density),

$$T_{eq} \propto \frac{V}{C_s Q_w}.$$

The sediment concentration reflects the erodibility of the land surface and is governed in large part by vegetation dynamics. It is a function of fire severity (because severity governs the extent of loss of soil-stabilizing vegetation; e.g., Benavides-Solorio & MacDonald, 2005), event sequencing (time between the fire and flood, which sets the extent of vegetation regrowth and resulting geomorphic stabilization that occurs between the two events), and efficiency of post-flood revegetation, which sets how quickly vegetation restabilizes the soil surface after the disturbance sequence.

Using this three-variable framework, we can define a conceptual parameter space of controls on  $T_{eq}$  for supply-limited landscapes (Figure 9).  $T_{eq}$  is lengthened by higher sediment supply and shortened by higher sediment concentrations in post-fire floods (due to higher soil erodibility caused by either more severe fire or shorter time between fire and flood) and higher-magnitude post-fire floods. Given that the primary effects of a fire–flood sequence are to increase land-surface erodibility by burning vegetation (fire) and to generate significant erosive stresses (flood), we expect that  $T_{eq}$  may be shorter in our study area than for many post-fire studies in which there was no major flood following the fire (e.g., Owens et al., 2013). One simplification inherent to this idea is that it assumes that  $V$ ,  $C_s$ , and  $Q_w$  are not correlated. For example, short recovery timescales may exist when rapid vegetation regrowth and soil stabilization reduce the functionally available sediment supply  $V$  by decreasing erodibility and therefore  $C_s$ —in other words, when sediment supply limitations are not fully realized because erodibility rapidly declines. Conversely, flooding (high  $Q_w$ ) might drive production of sediment (increased  $V$ )

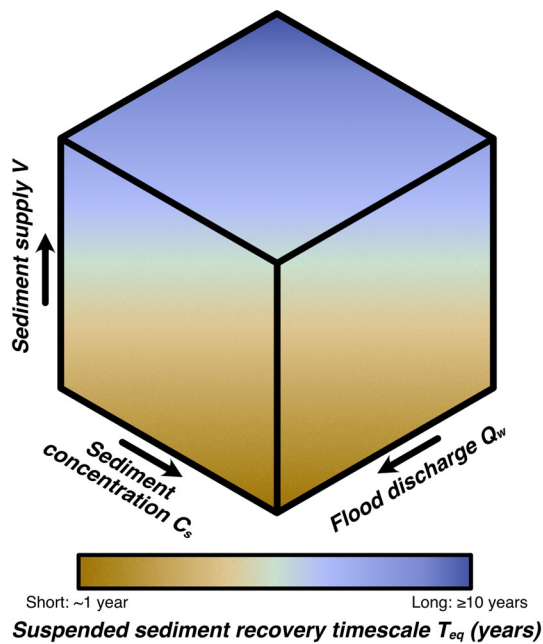


**FIGURE 9** Phase diagram conceptualizing the controls on the suspended-sediment recovery timescale for supply-limited landscapes. [Color figure can be viewed at [wileyonlinelibrary.com](https://onlinelibrary.wiley.com/doi/10.1002/rm.a.4236)]

that would not otherwise have been accessible to erosive flow events, potentially through debris flow, landsliding, or erosion of channel margins (e.g., Brogan, MacDonald, et al., 2019; Brogan, Nelson, & MacDonald, 2019; Cannon et al., 2008; Rengers et al., 2020).

Our study area may have experienced a relatively short  $T_{eq}$  because of a combination of the 2013 flood (high  $Q_w$ ), erodible sediment (high  $C_s$ ), and sediment supply limitation (low  $V$ ) (Figure 9). The flood helped accelerate post-fire recovery not only because it had high  $Q_w$  and high  $C_s$ —the latter due to its close temporal proximity to the fire—but also because it increased the erodibility of some of the remaining sediment (further increasing  $C_s$  for subsequent flows). Most of the available suspended sediment, which had been made more erodible by the effects of the flood, was exported by summer 2015. In our supply-limited region, a major post-fire flood accelerated suspended-sediment export, increasing peak SSCs and sediment loads early in the post-fire recovery process—a potential negative for managers—but reducing the duration of the post-fire disturbance. Our results suggest that the interplay between sediment supply and post-fire rainfall event sequencing sets post-fire suspended-sediment export. This is consistent with studies that include bedload in sediment yield estimates (e.g., East et al., 2021; Keller et al., 1997). Sediment availability and erosive event sequencing may therefore be important variables to explore when forecasting post-fire sediment dynamics (e.g., Sankey et al., 2017). Supply limitations may limit the sensitivity of our study landscape to changes in the fire regime (e.g., DiBiase & Lamb, 2013).

This study adds to a body of work with important implications for managing water quality and water infrastructure under ongoing climate change. Large volumes of suspended sediment transported by

post-fire floods can degrade water quality (e.g., Bladon et al., 2014; Smith et al., 2011) and exacerbate the ongoing problem of loss of water reservoir capacity through sedimentation (Randle et al., 2021). Predicted increases in fire severity and more extreme rainfall (USGCRP, 2023) will likely exacerbate the magnitude of post-fire suspended-sediment export and its negative impacts on water resources and infrastructure, at least in landscapes that are not very supply limited (East et al., 2022). Accumulating case studies documenting suspended-sediment export throughout fire–flood sequences aids the development of predictive, process-based models of post-fire sediment yield that can be used to elucidate landscape dynamics, forecast risks to infrastructure, and manage fire-prone ecosystems.

## 7 | CONCLUSIONS

We measured rainfall, streamflow, SSCs, and turbidity for 3 years after a severe fire in 2012, during which time a major flood occurred in the study area. This natural experiment provides a unique opportunity to investigate suspended-sediment dynamics throughout, and after, a fire–flood sequence. We find that post-fire summer storm SSCs declined year over year, while snowmelt runoff SSCs peaked in 2014 before declining in 2015. SSCs returned to background levels by 2015 for both seasons. As time elapsed, greater 30-minute rainfall intensities were required to generate a given SSC value during summer storms. Based on SSC, the time for the study area to recover from the 2012 fire was  $\sim 3$  years. Sediment loads declined slightly more slowly toward background values than did SSC due to higher snowmelt flows in 2014 and 2015, but  $\sim 3$  years also represents a plausible recovery period for sediment loads. A lack of post-2015 data precludes certainty that SSCs and loads remained near background values.

The 100-year flood that occurred  $\sim 15$  months after the fire, in addition to exporting 35 years' worth of suspended sediment, ushered in a long period ( $\sim 1.5$  years) of dramatically elevated sediment loads during both the snowmelt and summer seasons, due partially to higher flows in 2014 and 2015 than in 2013, and probably also due to resuspension of flood-deposited sediment. The flood therefore may have acted as an accelerant to watershed recovery. The year recovery timescale we interpret for our study area is consistent with the faster end-member of timescales inferred in prior post-fire recovery studies, likely due to the flushing effects of the flood and the supply-limited nature of the landscape in addition to some amount of soil stabilization by returning vegetation.

The timescale of suspended-sediment recovery from fire–flood sequences in supply-limited landscapes can be thought of as depending on sediment supply, relative sediment erodibility as governed by vegetation response to both fire severity and time elapsed between the fire and the flood, and the erosive stresses applied by the flood. In our case study, we interpret that suspended-sediment supply limitation, close temporal proximity of the fire and flood, and flood magnitude conspired to drive a more rapid return to baseline

suspended-sediment conditions than would be expected had there been no major flood.

While recovery of suspended-sediment transport to baseline conditions does not imply recovery of other aspects of watersheds (e.g., bedload transport, channel form), suspended-sediment dynamics are especially critical to water resource management; developing predictive power over suspended-sediment response to compound disturbances is an important research and management priority. Moving from conceptual (Figures 8 and 9) to predictive models of suspended-sediment dynamics throughout fire–flood sequences will require field data over longer time periods (5–10 years) and across a range of climate and vegetation regimes, geologic settings, fire intensities, and durations between fire and flood. Better understanding the controls on landscape response to fire–flood sequences will enable improved stewardship of land and water resources as climate change increases the frequency and severity of fires and floods throughout the western United States and elsewhere.

## ACKNOWLEDGEMENTS

The findings and conclusions in this publication are those of the authors and should not be construed to represent any official USDA or U.S. Government determination or policy. Any use of trade names is for descriptive purposes only and does not imply endorsement by the U.S. Government. This work was funded by the National Fire Plan through the U.S. Forest Service Rocky Mountain Research Station (to S. Ryan) and the Cities of Fort Collins and Greeley, CO (to S. Rathburn). Field and laboratory assistance was provided by Matt Schiff, Abbey Vogler, Jay Merrill, Mike Wyatt, Breanna Van, Aaron Blair, Josh Von Loh, and Nick Zilm, as well as the volunteers who constructed and dismantled the study sites. Tony Vorster and Miles Innes provided data on post-fire NDVI. Thanks to Rachel Glade, Allie Rhea, and Chuck Rhoades for helpful discussions. Reviews by Sharon Bywater-Reyes and two anonymous reviewers improved the manuscript.

## DATA AVAILABILITY STATEMENT

The streamflow, precipitation, turbidity, and suspended-sediment data collected for this study can be accessed at <https://doi.org/10.2737/RDS-2024-0028> through the U.S. Forest Service Research Data Archive (Ryan et al., 2024).

## ORCID

Charles M. Shobe  <https://orcid.org/0000-0003-3015-1283>

Sara L. Rathburn  <https://orcid.org/0000-0002-2514-4823>

## REFERENCES

- Ahrendt, S., Horner-Devine, A. R., Collins, B. D., Morgan, J. A., & Istanbuloglu, E. (2022). Channel conveyance variability can influence flood risk as much as streamflow variability in western Washington state. *Water Resources Research*, 58, e2021WR031890. <https://doi.org/10.1029/2021WR031890>
- Alessio, P., Dunne, T., & Morell, K. (2021). Post-wildfire generation of debris-flow slurry by rill erosion on colluvial hillslopes. *Journal of Geophysical Research - Earth Surface*, 126, e2021JF006108. <https://doi.org/10.1029/2021JF006108>
- Allan, R. P., & Soden, B. J. (2008). Atmospheric warming and the amplification of precipitation extremes. *Science*, 321, 1481–1484. <https://doi.org/10.1126/science.1160787>
- Anderson, S. W., Anderson, S. P., & Anderson, R. S. (2015). Exhumation by debris flows in the 2013 Colorado front range storm. *Geology*, 43, 391–394. <https://doi.org/10.1130/G36507.1>
- Andrews, E. D. (1984). Bed-material entrainment and hydraulic geometry of gravel-bed rivers in Colorado. *Geological Society of America Bulletin*, 95, 371–378. [https://doi.org/10.1130/0016-7606\(1984\)95<371:BEAHGO>2.0.CO;2](https://doi.org/10.1130/0016-7606(1984)95<371:BEAHGO>2.0.CO;2)
- Balch, J. K., Iglesias, V., Braswell, A. E., Rossi, M. W., Joseph, M. B., Mahood, A. L., Schrum, T. R., White, C. T., Scholl, V. M., McGuire, B., Karban, C., Buckland, M., & Travis, W. R. (2020). Social-environmental extremes: Rethinking extraordinary events as outcomes of interacting biophysical and social systems. *Earth's Future*, 8, e2019EF001319. <https://doi.org/10.1029/2019EF001319>
- Benavides-Solorio, J. D., & MacDonald, L. H. (2005). Measurement and prediction of post-fire erosion at the hillslope scale, Colorado front range. *International Journal of Wildland Fire*, 14, 457–474. <https://doi.org/10.1071/WF05042>
- Bladon, K. D., Emelko, M. B., Silins, U., & Stone, M. (2014). Wildfire and the future of water supply. *Environmental Science and Technology*, 48, 8936–8943. <https://doi.org/10.1021/es500130g>
- Brogan, D. J., MacDonald, L. H., Nelson, P. A., & Morgan, J. A. (2019). Geomorphic complexity and sensitivity in channels to fire and floods in mountain catchments. *Geomorphology*, 337, 53–68. <https://doi.org/10.1016/j.geomorph.2019.03.031>
- Brogan, D. J., Nelson, P. A., & MacDonald, L. H. (2019). Spatial and temporal patterns of sediment storage and erosion following a wildfire and extreme flood. *Earth Surface Dynamics*, 7, 563–590. <https://doi.org/10.5194/esurf-7-563-2019>
- Buma, B. (2015). Disturbance interactions: Characterization, prediction, and the potential for cascading effects. *Ecosphere*, 6, 1–17. <https://doi.org/10.1890/ES15-00058.1>
- Burned Area Emergency Response (BAER) Team. (2012). *High Park Fire Burned Area Emergency Response Report*, 35 p., produced in cooperation with the Colorado Dept. of Transportation, Larimer County, and U.S. Dept. of Agriculture: Natural Resources Conservation Service and Forest Service.
- Cai, L. (2006). Multi-response permutation procedure as an alternative to the analysis of variance: An SPSS implementation. *Behavior Research Methods*, 38, 51–59. <https://doi.org/10.3758/BF03192749>
- Cannon, S. H., Gartner, J. E., Wilson, R. C., Bowers, J. C., & Laber, J. L. (2008). Storm rainfall conditions for floods and debris flows from recently burned areas in southwestern Colorado and southern California. *Geomorphology*, 96, 250–269. <https://doi.org/10.1016/j.geomorph.2007.03.019>
- Cannon, S. H., Kirkham, R. M., & Parise, M. (2001). Wildfire-related debris-flow initiation processes, storm King Mountain, Colorado. *Geomorphology*, 39, 171–188. [https://doi.org/10.1016/S1069-555X\(00\)00108-2](https://doi.org/10.1016/S1069-555X(00)00108-2)
- Chow, A. T., Tsai, K.-P., Feghel, T. S., Pierson, D. N., & Rhoades, C. C. (2019). Lasting effects of wildfire on disinfection by-product formation in forested catchments. *Journal of Environmental Quality*, 48, 1826–1834. <https://doi.org/10.2134/jeq2019.04.0172>
- Dahm, C. N., Candelaria-Ley, R. I., Reale, C. S., Reale, J. K., & van Horn, D. J. (2015). Extreme water quality degradation following a catastrophic forest fire. *Freshwater Biology*, 60, 2584–2599. <https://doi.org/10.1111/fwb.12548>
- Dennison, P. E., Brewer, S. C., Arnold, J. D., & Moritz, M. A. (2014). Large wildfire trends in the western United States, 1984–2011. *Geophysical Research Letters*, 41, 2928–2933. <https://doi.org/10.1002/2014GL059576>

- DiBiase, R. A., & Lamb, M. P. (2013). Vegetation and wildfire controls on sediment yield in bedrock landscapes. *Geophysical Research Letters*, 40, 1093–1097. <https://doi.org/10.1002/grl.50277>
- Diek, S., Temme, A. J. A. M., & Teuling, S. J. (2014). The effect of spatial soil variation on the hydrology of a semi-arid Rocky Mountains catchment. *Geoderma*, 235–236, 113–126. <https://doi.org/10.1016/j.geoderma.2014.06.028>
- East, A. E., Logan, J. B., Dartnell, P., Lieber-Kotz, O., Cavagnaro, D. B., McCoy, S. W., & Lindsay, D. N. (2021). Watershed sediment yield following the 2018 Carr fire, Whiskeytown National Recreation Area, northern California. *Earth and Space Science*, 8, e2021EA001828. <https://doi.org/10.1029/2021EA001828>
- East, A. E., Warrick, J. A., Li, D., Sankey, J. B., Redsteer, M. H., Gibbs, A. E., Coe, J. A., & Barnard, P. L. (2022). Measuring and attributing sedimentary and geomorphic responses to modern climate change: Challenges and opportunities. *Earth's Future*, 10, e2022EF002983. <https://doi.org/10.1029/2022EF002983>
- Ebel, B. A., Moody, J. A., & Martin, D. A. (2012). Hydrologic conditions controlling runoff generation immediately after wildfire. *Water Resources Research*, 48, W03529. <https://doi.org/10.1029/2011WR011470>
- Eidenshink, J., Schwind, B., Brewer, K., Zhu, Z.-L., Quayle, B., & Howard, S. (2007). A project for monitoring trends in burn severity. *Fire Ecology*, 3, 3–21. <https://doi.org/10.4996/fireecology.0301003>
- Elliott, J. G. (1988). Regionalization of mean annual suspended-sediment loads in streams, central, northwestern, and southwestern Colorado. U.S. Geological Survey Water-Resources Investigations Report 87–4193. <https://doi.org/10.3133/wri874193>
- Elliott, J. G., & DeFeyer, K. L. (1986). Sediment data sources and estimated annual suspended-sediment loads of rivers and streams in Colorado. U.S. Geological Survey Water-Resources Investigations Report 86–4344. <https://doi.org/10.3133/wri864344>
- Florsheim, J. L., Chin, A., Kinoshita, A. M., & Nourbakhshbeidokhti, S. (2017). Effect of storms during drought on post-wildfire recovery of channel sediment dynamics and habitat in the southern California chaparral, USA. *Earth Surface Processes and Landforms*, 42, 1482–1492. <https://doi.org/10.1002/esp.4117>
- Fryirs, K. (2017). River sensitivity: A lost foundation concept in fluvial geomorphology. *Earth Surface Processes and Landforms*, 42, 55–70. <https://doi.org/10.1002/esp.3940>
- Gochis, D., Schumacher, R., Friedrich, K., Doesken, N., Kelsch, M., Sun, J., Ikeda, K., Lindsey, D., Wood, A., Dolan, B., Matrosov, S., Newman, A., Mahoney, K., Rutledge, S., Johnson, R., Kucera, P., Kennedy, P., Sempere-Torres, D., Steiner, M., ... Brown, B. (2015). The great Colorado flood of September 2015. *Bulletin of the American Meteorological Society*, 96, 1461–1487. <https://doi.org/10.1175/BAMS-D-13-00241.1>
- Goode, J. R., Luce, C. H., & Buffington, J. M. (2012). Enhanced sediment delivery in a changing climate in semi-arid mountain basins: Implications for water resource management and aquatic habitat in the northern Rocky Mountains. *Geomorphology*, 139–140, 1–15. <https://doi.org/10.1016/j.geomorph.2011.06.021>
- Green, G. N. (1992). The digital geologic map of Colorado in ARC/INFO format. U.S. Geological Survey Open-File Report 92-507-D-O. <https://doi.org/10.3133/ofr92507DO>
- Guillinger, J. J., Gray, A. B., Barth, N. C., & Fong, B. T. (2020). The evolution of sediment sources over a sequence of postfire sediment-laden flows revealed through repeat high-resolution change detection. *Journal of Geophysical Research - Earth Surface*, 125, e2020JF005527. <https://doi.org/10.1029/2020JF005527>
- Interagency Committee on Water Data. (1982). Guidelines for determining flood flow frequency. In *Hydrology subcommittee bulletin 17B*. Reston, VA.
- Jong-Levinger, A., Banerjee, T., Houston, D., & Sanders, B. F. (2022). Compound post-fire flood hazards considering infrastructure sedimentation. *Earth's Future*, 10, e2022EF002670. <https://doi.org/10.1029/2022EF002670>
- Jumps, N., Gray, A. B., Guillinger, J. J., & Cowger, W. C. (2022). Wildfire impacts on the persistent suspended sediment dynamics of the Ventura River, California. *Journal of Hydrology: Regional Studies*, 41, 101096. <https://doi.org/10.1016/j.jrh.2022.101096>
- Kampf, S. K., Brogan, D. J., Schmeer, S., MacDonald, L. H., & Nelson, P. A. (2016). How do geomorphic effects of rainfall vary with storm type and spatial scale in a post-fire landscape? *Geomorphology*, 273, 39–51. <https://doi.org/10.1016/j.geomorph.2016.08.001>
- Keller, E. A., Valentine, D. W., & Gibbs, D. R. (1997). Hydrological response of small watersheds following the southern California painted cave fire of June 1990. *Hydrological Processes*, 11, 401–414. [https://doi.org/10.1002/\(SICI\)1099-1085\(19970330\)11:4<401::AID-HYP447>3.0.CO;2-P](https://doi.org/10.1002/(SICI)1099-1085(19970330)11:4<401::AID-HYP447>3.0.CO;2-P)
- Lane, P. N., Sheridan, G. J., & Noske, P. J. (2006). Changes in sediment loads and discharge from small mountain catchments following wildfire in south eastern Australia. *Journal of Hydrology*, 331, 495–510. <https://doi.org/10.1016/j.jhydrol.2006.05.035>
- Lanini, J. S., Clark, E. A., & Lettenmaier, D. P. (2009). Effects of fire-precipitation timing and regime on post-fire sediment delivery in Pacific northwest forests. *Geophysical Research Letters*, 36, L01402. <https://doi.org/10.1029/2008GL034588>
- Larsen, I. J., MacDonald, L. H., Brown, E., Rough, D., Welsh, M. J., Pietraszek, J. H., Libohova, Z., Benavides-Solorio, J. D., & Schaffrath, K. (2009). Causes of post-fire runoff and erosion: Water repellency, cover, or soil sealing? *Soil Science Society of America Journal*, 73, 1393–1407. <https://doi.org/10.2136/sssaj2007.0432>
- Lewis, J., & Eads, R. (2009). Implementation guide for turbidity threshold sampling: Principles, procedures, and analysis. General Technical Report PSW-GTR-212. <https://doi.org/10.2737/PSW-GTR-212>
- Malmon, D. V., Reneau, S. L., Katzman, D., Lavine, A., & Lyman, J. (2007). Suspended sediment transport in an ephemeral stream following wildfire. *Journal of Geophysical Research*, 112, F02006. <https://doi.org/10.1029/2005JF000459>
- Martin, D. A. (2016). At the nexus of fire, water, and society. *Philosophical Transactions of the Royal Society B*, 371, 20150172. <https://doi.org/10.1098/rstb.2015.0172>
- McGuire, L. A., Rengers, F. K., Kean, J. W., & Staley, D. M. (2017). Debris flow initiation by runoff in a recently burned basin: Is grain-by-grain sediment bulking or mass failure to blame? *Geophysical Research Letters*, 44, 7310–7319. <https://doi.org/10.1002/2017GL074243>
- Mielke, P. W., & Berry, K. J. (2007). *Permutation methods: A distance function approach* (2nd ed.). Springer-Verlag.
- Miller, S., Rhodes, C., Robichaud, P., Ryan, S., Kovacs, J., Chambers, C., Rathburn, S., Heath, J., Kampf, S., Wilson, C., Brogan, D., Piehl, B., Miller, M.E., Giordanengo, J., Berryman, E., & Rocca, M. (2017). Learn from the burn: The High Park Fire 5 years later. In *Science you can use bulletin*, issue 25. Rocky Mountain Research Station, 18 pp.
- Montgomery, D. R., & Buffington, J. M. (1997). Channel-reach morphology in mountain drainage basins. *Geological Society of America Bulletin*, 109, 596–611. [https://doi.org/10.1130/0016-7606\(1997\)109<0596:CRMIMD>2.3.CO;2](https://doi.org/10.1130/0016-7606(1997)109<0596:CRMIMD>2.3.CO;2)
- Moody, J. A., & Martin, D. A. (2001). Initial hydrologic and geomorphic response following a wildfire in the Colorado front range. *Earth Surface Processes and Landforms*, 26, 1049–1070. <https://doi.org/10.1002/esp.253>
- Moody, J. A., & Martin, D. A. (2009). Forest fire effects on geomorphic processes. In A. Cerda & P. R. Robichaud (Eds.), *Fire effects on soils and restoration strategies* (pp. 41–79). CRC Press.
- Moody, J. A., Martin, D. A., & Cannon, S. H. (2008). Post-wildfire erosion response in two geologic terrains in the western USA. *Geomorphology*, 95, 103–118. <https://doi.org/10.1016/j.geomorph.2007.05.011>
- Morris, S. E., & Moses, T. A. (1987). Forest fire and the natural soil erosion regime in the Colorado front range. *Annals of the American Association of Geographers*, 77, 245–254.

- Murphy, S. F., McCleskey, R. B., & Martin, D. A. (2015). The role of precipitation type, intensity, and spatial distribution in source water quality after wildfire. *Environmental Research Letters*, *10*, 084007. <https://doi.org/10.1088/1748-9326/10/8/084007>
- Nolan, K. M., & Shields, R. R. (2000). Measurement of stream discharge by wading. U.S. Geological Survey water-resources investigations report 2000-4036. <https://doi.org/10.3133/wri20004036>
- Oliver, A. A., Reuter, J. E., Heyvaert, A. C., & Dahlgran, R. A. (2012). Water quality response to the angora fire, Lake Tahoe, California. *Biogeochemistry*, *111*, 361-376. <https://doi.org/10.1007/s10533-011-9657-0>
- Owens, P. N., Giles, T. R., Petticrew, E. L., Leggat, M. S., Moore, R. D., & Eaton, B. C. (2013). Muted responses of streamflow and suspended sediment flux in a wildfire-affected watershed. *Geomorphology*, *202*, 128-139. <https://doi.org/10.1016/j.geomorph.2013.01.001>
- Patton, A. I., Rathburn, S. L., Bilderback, E. L., & Lukens, C. E. (2018). Patterns of debris flow initiation and periglacial sediment sourcing in the Colorado front range. *Earth Surface Processes and Landforms*, *43*, 2998-3008. <https://doi.org/10.1002/esp.4463>
- Petticrew, E. L., Owens, P. N., & Giles, T. R. (2006). Wildfire effects on the quantity and composition of suspended and gravel-stored sediments. *Water, Air, & Soil Pollution: Focus*, *6*, 647-656. <https://doi.org/10.1007/s11267-006-9049-y>
- Phillips, J. D., & van Dyke, C. (2016). Principles of geomorphic disturbance and recovery in response to storms. *Earth Surface Processes and Landforms*, *41*, 971-979. <https://doi.org/10.1002/esp.3912>
- Randle, T. J., Morris, G. L., Tullios, D. D., Weirich, F. H., Kondolf, G. M., Moriasi, D. N., Annandale, G. W., Fripp, J., Minear, J. T., & Wegner, D. L. (2021). Sustaining United States reservoir storage capacity: Need for a new paradigm. *Journal of Hydrology*, *602*, 126686. <https://doi.org/10.1016/j.jhydrol.2021.126686>
- Rasmussen, P. P., Gray, J. R., Glysson, G. D., & Ziegler, A. C. (2009). Guidelines and procedures for computing time-series suspended-sediment concentrations and loads from in-stream turbidity-sensor and streamflow data. U.S. Geological Survey Techniques and Methods Book 3, chap. C4.
- Rathburn, S. L., Shahverdian, S. M., & Ryan, S. E. (2018). Post-disturbance sediment recovery: Implications for watershed resilience. *Geomorphology*, *305*, 61-75. <https://doi.org/10.1016/j.geomorph.2017.08.039>
- Reale, J. K., van Horn, D. J., Condon, K. E., & Dahm, C. N. (2015). The effects of catastrophic wildfire on water quality along a river continuum. *Freshwater Science*, *34*, 1426-1442. <https://doi.org/10.1086/684001>
- Rengers, F. K., McGuire, L. A., Kean, J. W., Staley, D. M., Dobre, M., Robichaud, P. R., & Swetnam, T. (2021). Movement of sediment through a burned landscape: Sediment volume observations and model comparisons in the San Gabriel Mountains, California, USA. *Journal of Geophysical Research - Earth Surface*, *126*, e2020JF006053. <https://doi.org/10.1029/2020JF006053>
- Rengers, F. K., McGuire, L. A., Oakley, N. S., Kean, J. W., Staley, D. M., & Tang, H. (2020). Landslides after wildfire: Initiation, magnitude, and mobility. *Landslides*, *17*, 2631-2641. <https://doi.org/10.1007/s10346-020-01506-3>
- Rhoades, C. C., Entwistle, D., & Butler, D. (2011). The influence of wildfire extent and severity on streamwater chemistry, sediment and temperature following the Hayman fire, Colorado. *International Journal of Wildland Fire*, *20*, 430-442. <https://doi.org/10.1071/WF09086>
- Richer, E. (2009). *Snowmelt runoff analysis and modeling for the upper cache La Poudre Basin, Colorado*. M.S. Thesis. Colorado State University.
- Ryan, S. E., Dixon, M. K., & Dwire, K. A. (2006). The use of turbidity sensors for monitoring sediment loads following wildfire. In *Proceedings of the Eighth Interagency Sedimentation and Third Interagency Hydrologic Modeling Conference* (pp. 378-385). Subcommittee on Sedimentation.
- Ryan, S. E., Dwire, K. A., & Dixon, M. K. (2011). Impacts of wildfire on runoff and sediment loads at little Granite Creek, western Wyoming. *Geomorphology*, *129*, 113-130. <https://doi.org/10.1016/j.geomorph.2011.01.017>
- Ryan, S. E., Porth, L. S., & Troendle, C. A. (2005). Coarse sediment transport in mountain streams in Colorado and Wyoming, USA. *Earth Surface Processes and Landforms*, *30*, 269-288. <https://doi.org/10.1002/esp.1128>
- Ryan, S. E., Shobe, C. M., Rathburn, S. L., & Dixon, M. K. (2024). *Data on fluvial suspended-sediment response to wildfire and a major post-fire flood [dataset]*. Forest Service Research Data Archive. <https://doi.org/10.2737/RDS-2024-0028>
- Salant, N. L., Hassan, M. A., & Alonso, C. V. (2007). Suspended sediment dynamics at high and low storm flows in two small watersheds. *Hydrological Processes*, *22*, 1573-1587. <https://doi.org/10.1002/hyp.6743>
- Sanderson, B. M., Wobus, C., Mills, D., Zarakas, C., Crimmins, A., Sarofim, M. C., & Weaver, C. (2019). Informing future risks of record-level rainfall in the United States. *Geophysical Research Letters*, *46*, 3963-3972. <https://doi.org/10.1029/2019GL082362>
- Sankey, J. B., Kreidler, J., Hawbaker, T. J., McVay, J. L., Miller, M. E., Mueller, E. R., Vaillant, N. M., Lowe, S. E., & Sankey, T. T. (2017). Climate, wildfire, and erosion ensemble foretells more sediment in western USA watersheds. *Geophysical Research Letters*, *44*, 8884-8894. <https://doi.org/10.1002/2017GL073979>
- Scott, D. F., Curran, M. P., Robichaud, P. R., & Wagenbrenner, J. W. (2009). Soil erosion after forest fire. In A. Cerda & P. R. Robichaud (Eds.), *Fire effects on soils and restoration strategies* (pp. 177-195). CRC Press.
- Shahverdian, S. M. (2015). *Controls on post-High Park fire channel response, south fork cache La Poudre Basin, Colorado*. M.S. Thesis. Colorado State University.
- Silins, U., Stone, M., Emelko, M. B., & Bladon, K. D. (2009). Sediment production following severe wildfire and post-fire salvage logging in the Rocky Mountain headwaters of the Oldman River basin, Alberta. *Catena*, *79*, 189-197. <https://doi.org/10.1016/j.catena.2009.04.001>
- Smith, H. G., Sheridan, G. J., Lane, P. N. J., Nyman, P., & Haydon, S. (2011). Wildfire effects on water quality in forest catchments: A review with implications for water supply. *Journal of Hydrology*, *396*, 170-192. <https://doi.org/10.1016/j.jhydrol.2010.10.043>
- USGCRP. (2023). In A. R. Crimmins, C. W. Avery, D. R. Easterling, K. E. Kunkel, B. C. Stewart, & T. K. Maycock (Eds.), *Fifth National Climate Assessment*. U.S. Global Change Research Program. <https://doi.org/10.7930/NCA5.2023>
- Veblen, T. T., & Donnegan, J. A. (2005). Historical range of variability for forest vegetation of the National Forests of the Colorado Front Range. Final Report: USDA Forest Service Agreement No. 1102-0001-99-033, USDA Forest Service, Rocky Mountain Region, Golden, CO.
- Warrick, J. A., Hatten, J. A., Pasternack, G. B., Gray, A. B., Goni, M. A., & Wheatcroft, R. A. (2012). The effects of wildfire on the sediment yield of a coastal California watershed. *Geological Society of America Bulletin*, *124*, 1130-1146. <https://doi.org/10.1130/B30451.1>
- Warrick, J. A., Vos, K., East, A. E., & Vitousek, S. (2022). Fire (plus) flood (equals) beach: Coastal response to an exceptional sediment discharge event. *Scientific Reports*, *12*, 3848. <https://doi.org/10.1038/s41598-022-07209-0>
- Westerling, A. L., Hidalgo, H. G., Cayan, D. R., & Swetnam, T. W. (2006). Warming and earlier spring increase Western U.S. forest wildfire activity. *Science*, *313*, 940-943. <https://doi.org/10.1126/science.1128834>
- Wilson, C., Kampf, S. K., Ryan, S., Covino, T., MacDonald, L. H., & Gleason, H. (2020). Connectivity of post-fire runoff and sediment from nested hillslopes and watersheds. *Hydrological Processes*, *35*, e13975. <https://doi.org/10.1002/hyp.13975>
- Wohl, E., Marshall, A., Scamardo, J., & Rathburn, S. (2023). Biogeomorphic processes, spatial heterogeneity, and river corridor resilience to stand-killing wildfire. *Geological Society of America Special Paper*, *562*. [https://doi.org/10.1130/2024.2562\(08\)](https://doi.org/10.1130/2024.2562(08))



Writer, J. H., Hohner, A., Oropeza, J., Schmidt, A., Cawley, K. M., & Rosario-Ortiz, F. L. (2014). Water treatment implications after the High Park wildfire, Colorado. *Journal - American Water Works Association*, 106, E189–E199. <https://doi.org/10.5942/jawwa.2014.106.0055>

### SUPPORTING INFORMATION

Additional supporting information can be found online in the Supporting Information section at the end of this article.

**How to cite this article:** Ryan, S. E., Shobe, C. M., Rathburn, S. L., & Dixon, M. K. (2024). Suspended-sediment response to wildfire and a major post-fire flood on the Colorado Front Range. *River Research and Applications*, 1–17. <https://doi.org/10.1002/rra.4286>